

Anomalous Fano Profiles in External Fields

Alejandro Zielinski^a, Vinay Pramod Majety^a, Stefan Nagele^b,
Renate Pazourek^b, Joachim Burgdörfer^b, and Armin Scrinzi^{a*}

^aPhysics Department, Ludwig Maximilians Universität, D-80333 Munich, Germany and
^bInstitute for Theoretical Physics, Vienna University of Technology, Vienna, Austria

(Dated: April 27, 2022)

We show that external control of Fano resonances in general leads to complex Fano q -parameters. Fano line shapes of photo-electron and transient absorption spectra in presence of an infrared control field are investigated. Computed transient absorption spectra are compatible with a recent experiment [C. Ott *et al.*, Science 340, 716 (2013)] but suggest a modification of the interpretation proposed there. Control mechanisms for photo-electron spectra are exposed: control pulses applied *during* excitation modify the line shapes by momentum boosts of the continuum electrons. Pulses arriving *after* excitation generate interference fringes due to infrared two-photon transitions.

PACS numbers:

The celebrated Fano formula [1]

$$\sigma(\Delta E) = \sigma_0 \frac{|q\Gamma + 2\Delta E|^2}{\Gamma^2 + (2\Delta E)^2} \quad (1)$$

describes the modulation of the cross section of any excitation process to a continuum that is structured by a single embedded resonant state compared to the smooth background cross section σ_0 in absence of the embedded state. Apart from the resonance width Γ and the detuning ΔE there appears the q parameter, which produces a characteristic asymmetry and — if it is real — an exact zero of the cross section. The Fano profile is one of the prominent manifestations of quantum mechanical interference in scattering. The mechanism is ubiquitous and independent of the particular nature of the transitions involved. In recent years it was proposed to control the line shape by external fields and interactions, and schemes in diverse fields of physics were experimentally realized (see review in [2]). For a quantum dot system controlled by a time-independent magnetic field it was observed that a generalization to complex q was required to fit the control-dependence of the line shape. Complex values of q result from the breaking of time-reversal symmetry by the magnetic field [3]. In contrast, in standard Fano theory [1], applicable to time-reversal symmetric systems, q is real-valued (see, e.g., [4]). Complex q has also been discussed as a signature of dephasing and decoherence in atoms [5, 6] as well as in quantum dots [7] and microwave cavities [8]. More generally, complex q are expected to appear whenever coupling to the environment or external fields turn the embedded state into a state that cannot be described by a real-valued eigenfunction.

In this Letter we show that also a time-dependent electric control field, specifically an infrared (IR) probe pulse, generates complex q -parameters. Recently, the control of the line shape of transient absorption spectra (TAS) arising in a pump-probe scenario for helium was demonstrated [9]: the excitation of the $2snp$ series of doubly excited states by a short extreme ultraviolet (XUV) pulse

was probed by a weak, time-delayed near-IR pulse. The modulation of TAS line shapes was described as a control of a real valued Fano q parameter through an IR induced phase shift. Here we present *ab initio* numerical solutions that show that TAS as well as photo-electron spectra (PES) are characterized by complex rather than real q . For PES we expose the two main mechanisms underlying the appearance of a non-zero imaginary part of q using a generalized Fano model that includes an external control. First, we show that the phase shift discussed in [9] directly leads to complex q in PES. However, a second mechanism dominates the PES line shapes when XUV and IR pulses overlap: the free electron momenta are boosted by

$$\vec{k} \rightarrow \vec{k} + \vec{A}(t_0), \quad \vec{A}(t_0) := - \int_{t_0}^{t_1} d\tau \vec{\mathcal{E}}(\tau), \quad (2)$$

from their values after XUV excitation time t_0 until the end of the IR field $\vec{\mathcal{E}}(t)$ at time t_1 . (Unless indicated otherwise, we use atomic units, where electron mass, proton charge, and \hbar are all set equal to 1.) The boost redistributes amplitudes among the partial waves and modifies the Fano interference of the embedded state with the continuum in the $l = 1$ decay channel. Both mechanisms conserve the universal Fano line-shape Eq. (1), albeit with complex q .

An important higher order process that leads to a departure from the Fano profile is two-IR-photon coupling, which was discussed for a multiplet of embedded states [10] and for Autler-Townes splitting [11]. In the present setting, two-IR-photon coupling generates characteristic interference-like modulations of the PES when the XUV and IR pulses are well-separated in time. Similar structures will appear when the decaying state is partially depleted by a delayed IR [12]. The importance of non-resonant IR multi-photon processes in the excitation of dipole-forbidden auto-ionizing states was noted recently [13].

We first present the PES in the vicinity of the He(2s2p)

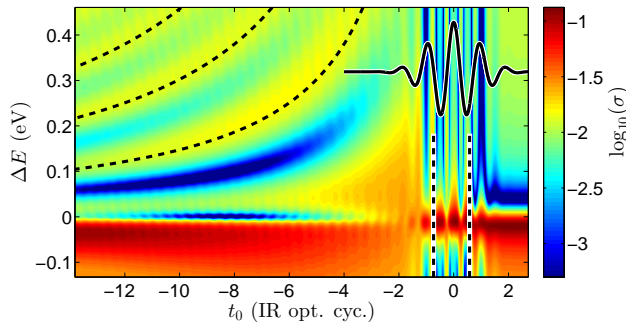


FIG. 1: PES $\sigma(\Delta E)$ in the vicinity of the $2s2p$ resonance as a function of XUV excitation time t_0 ($l = 1$ partial wave). IR peak intensity $2 \times 10^{12} \text{ W/cm}^2$. Solid line: IR field, curved fine-dashed lines: $2n\pi\hbar/|t_0|$, $n = 1, 2, 3$, closely follow interference maxima. Negative t_0 correspond to the XUV preceding IR. Dashed vertical lines indicate the lineout times of Fig. 2.

line as a function of XUV excitation time t_0 with an IR pulse centered at $t = 0$ (Fig. 1). The results were obtained by numerically solving the time-dependent Schrödinger equation of the He atom in full 3+3 spatial dimensions. Spectra were computed using the time-dependent surface flux method (tSURFF, [14, 15]). For a summary of the computational approach and discussion of its accuracy, see [16]. The XUV center wavelength of $\lambda = 21 \text{ nm}$ was chosen to match the excitation to the $2s2p$ state, but the spectral width of $\sim 10 \text{ eV}$ at the pulse duration of 0.15 fs evenly covers the entire $2snp$ series of doubly excited He states. The calculations were performed for IR wavelength of 800 nm with a pulse duration of 2 optical cycles, peak intensity $2 \times 10^{12} \text{ W/cm}^2$, and parallel linear polarization of the XUV and IR pulses.

The two lineouts (Fig. 2) pertain to $t_0 = -3/4$ and $+1/2$ (in units of IR optical cycle). At $t_0 = -3/4$, where the XUV pulse coincides with a node of the IR electric field, one sees a strongly asymmetric Fano profile. In contrast, at $t = +1/2$, peak of the IR field, the profile is Lorentz-like. Neither the width nor the position of the resonance are affected by the weak IR. The pattern is repeated as t_0 is scanned through the IR pulse.

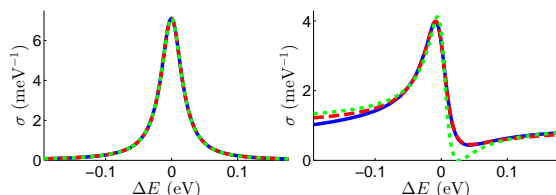


FIG. 2: PES at two different delay times as indicated in Fig. 1. Left: $t_0 = 1/2$ IR opt.cyc., near a field peak, right: $t_0 = -3/4$, near a field node. IR peak intensity 10^{12} W/cm^2 . Solid: numerical result, dashed: fit admitting complex q , dot-dashed: fit with q restricted to real. All three lines nearly coincide at $t_0 = 1/2$.

Fig. 2 also contains fits to the lines by Eq. (1), where Γ was taken from the IR-free case. Only the overall intensity σ_0 and the q -parameter and were adjusted, either restricting q to real values and or admitting complex q , respectively. When the XUV coincides with a node of the IR (right panel of Fig. 2), only the fit with complex q is satisfactory: there is no exact zero in the spectrum when IR and XUV pulse overlap, which trivially rules out an accurate fit by Eq. (1) with real q .

For the example of PES we show how complex q arises in the framework of a generalized Fano theory. A standard Fano Hamiltonian has the form

$$H = |\varphi\rangle E_\varphi \langle\varphi| + \int |\vec{k}\rangle \frac{k^2}{2} \langle\vec{k}| + |\vec{k}\rangle V_{\vec{k}} \langle\varphi| + |\varphi\rangle V_{\vec{k}}^* \langle\vec{k}| d^3k, \quad (3)$$

where the embedded bound state $|\varphi\rangle$ interacts with the continuum states $|\vec{k}\rangle$ through $V_{\vec{k}} = \langle\vec{k}|V|\varphi\rangle$. Solutions are known for the exact scattering eigenfunctions $|\xi_{\vec{k}}\rangle$, the resonance width Γ , and the shift of the resonance position from the non-interacting E_φ . The Fano transition amplitude $\langle\xi_{\vec{k}}|T|\phi_0\rangle$ for an arbitrary transition operator T from some initial state $|\phi_0\rangle$ leads to the Fano cross section (1). We introduce the wave packet after transition

$$T|\phi_0\rangle =: |\psi_0\rangle = |\varphi\rangle X_\varphi + \int d^3k |\vec{k}\rangle X_{\vec{k}}, \quad (4)$$

with the transition amplitudes from the initial state $X_\varphi = \langle\varphi|T|\phi_0\rangle$ and $X_{\vec{k}} = \langle\vec{k}|T|\phi_0\rangle$. For notational simplicity we consider the case where $|\varphi\rangle$ decays into a well-defined angular momentum state, in case of the $2s2p$ doubly excited state this is the $l = 1$ partial wave. The q -parameter for the standard Fano Hamiltonian (3), denoted as q_0 , is

$$q_0 = \frac{1}{\pi V_{\vec{k}}^* k} \frac{\langle\varphi|\psi_0\rangle + \mathcal{P} \int k'^2 dk' \frac{2V_{\vec{k}}^*}{k^2 - k'^2} \langle k'|\psi_0\rangle}{\langle k|\psi_0\rangle}, \quad (5)$$

where the $|k\rangle$ denotes the $l = 1$ partial wave continuum states with $k = \sqrt{k^2}$ and $V_{\vec{k}}$ are the coupling matrix elements between embedded and continuum states. When the $\langle k'|\psi_0\rangle$ and $\langle\varphi|\psi_0\rangle$ all share the same phase, q is real.

In our model for the transition in the pulse overlap region, we assume that the initial state $|\phi_0\rangle$ is unaffected by the IR and that the effect on the embedded state $|\varphi\rangle$ is only a Stark shift $\Delta E_\varphi(t)$ relative to the field-free energy E_φ . The interaction of the IR with the continuum states is described in the standard “strong field approximation” [17]: when the IR field prevails over the atomic potential, the continuum states at time t can be approximated as plane waves with wave vector $\vec{k} - \vec{A}(t)$ and the phase of the time-evolution is modified accordingly. Finally, we assume that the IR pulse duration is short compared to the decay time of the embedded state. With that the net effect of the IR pulse is to replace $|\psi_0\rangle$ by a modified initial wave packet

$$|\psi_1\rangle = |\varphi\rangle X_\varphi + \int d^3k e^{-i\Phi_{\vec{k}}} |\vec{k}\rangle X_{\vec{k} - \vec{A}(t_0)} \quad (6)$$

(see Supplemental Material [18]). The phase offset $\Phi_{\vec{k}}$ between embedded and continuum states accumulated from excitation at t_0 until the end of the IR pulse at t_1 , $\vec{A}(t_1) = 0$, is

$$\Phi_{\vec{k}} = \int_{t_0}^{t_1} d\tau \left([\vec{k} - \vec{A}(\tau)]^2/2 - E_\varphi - \Delta E_\varphi(\tau) \right). \quad (7)$$

Clearly, even if the initial amplitudes X_φ and $X_{\vec{k}-\vec{A}(t_0)}$ are all real, the interaction with the IR imprints a phase-modulation on $|\psi_1\rangle$ and the Fano parameter becomes complex. Moreover, in $X_{\vec{k}-\vec{A}(t_0)}$ the partial waves are redistributed compared to the IR-free $X_{\vec{k}}$ by the addition of a streaking momentum $\vec{A}(t_0)$. A short calculation (see [18]) leads to the IR modification of the Fano parameter

$$q_1 = q_0 + a \left(e^{-i\chi} / \mathcal{J} - 1 \right), \quad (8)$$

where $a = \langle \varphi | \psi_0 \rangle / (\pi V_{\vec{k}}^* k \langle k | \psi_0 \rangle)$ denotes the ratio of embedded to continuum amplitudes without the IR, and

$$\chi = \int_{t_0}^{t_1} d\tau \left[\Delta E_\varphi(\tau) - \vec{A}^2(\tau)/2 \right] \quad (9)$$

is a laser-induced phase shift between the two components. Although the phase-shift χ does give a numerically discernable contribution, the t_0 -dependence of q_1 is dominated by

$$\mathcal{J} = j_0(|\vec{\alpha}|k) - 2j_2(|\vec{\alpha}|k) - 3i \frac{j_1(|\vec{\alpha}|k)}{|\vec{\alpha}|k} \vec{\alpha} \cdot \vec{A}(t_0), \quad (10)$$

where the spatial offset of a free electron by the IR pulse

$$\vec{\alpha} = \int_{t_0}^{t_1} d\tau \vec{A}(\tau) \quad (11)$$

appears in the argument of the spherical Bessel functions j_l . The \mathcal{J} -term accounts for streaking by the term $\int_{t_0}^{t_1} \vec{k} \cdot \vec{A}(\tau) d\tau$ in $\Phi_{\vec{k}}$. By the dipole selection rule $|\psi_0\rangle$ has angular momentum $l = 1$ and therefore only the j_0 , j_1 , and j_2 contribute to the $l = 1$ partial wave emission.

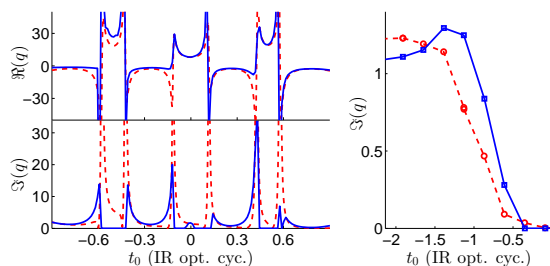


FIG. 3: Dependence of q_1 on XUV-IR delay time t_0 according to Eq. (8) (dashed lines) and from fits to numerical results (solid lines). Upper panel: $\Re(q_1)$, lower panel: $\Im(q_1)$. Right: $\Im(q_1)$ at times t_n near the nodes of the field ($\vec{\alpha} = 0$, see text): Eq. (8) (bullets) and fit (squares).

In Fig. 3 we compare Eq. (8) with fits to the numerically computed 2s2p line. For the fits, the amplitude ratio was kept constant at the field-free value of $a = -3.3$ and Stark shifts were neglected, $\Delta E_\varphi \equiv 0$. Sign changes of the real part and peaks in the imaginary parts are all well reproduced. Quantitative deviations must be expected in the strong field approximation, for example, due to the use of plane waves $|\vec{k}\rangle$ instead of the exact scattering solutions. In addition, there is a non-negligible IR two-photon coupling, as will be discussed below.

There are excitation times $t_0 = t_n$ where the spatial offset vanishes, $\vec{\alpha} = 0$, and therefore $\mathcal{J} = 1$. At these delays, the imaginary part of q_1 is exclusively due to the phase-shifts χ . Up to small corrections arising from the short IR pulse duration, the t_n coincide with zeros of the field. At the t_n the profile is Fano-like (Fig. 2), except that the characteristic minimum remains slightly above zero. In our model, the minima for subsequent t_n 's grow monotonically as the delay $|t_0|$ increases (Fig. 3, right panel) reflecting the accumulation of the shift χ , Eq. (9). For overlapping pulses, all resonances 2snp, $n = 2$ through 7 show the same delay-dependence, which corroborates that line-shape modulations are dominated by the dressing of the continuum.

When the XUV precedes the IR pulse without overlap (large negative t_0), the spatial offset goes to zero ($\vec{\alpha} \approx 0$) and therefore $\mathcal{J} \approx 1$. Here, line-shapes are the combined effect of the phase-shift χ and IR two-photon coupling between embedded and continuum states. Two-photon coupling is not included in the standard Fano model Eq. (3). It manifests itself in side-band like interferences. Stimulated 2-IR-photon emission creates ripples in the otherwise smooth non-resonant PES around the energies $E_- = E_\varphi - 2\omega$, where ω is the IR photon energy. The electron amplitude generated by two-photon absorption near $E_+ = E_\varphi + 2\omega$ is super-imposed with the higher-lying Fano resonances and therefore not clearly discernable. Absorption-emission transitions couple the embedded state to the continuum near $E = E_\varphi$. We model the spectral features near E_β , $\beta = \varphi$ and $\beta = -$ by

$$\sigma(E) = |f(E) + \mathcal{E}_0^2 e^{-it_0(E-E_\beta)} b_\beta(E)|^2, \quad (12)$$

where t_0 is the XUV-IR delay, \mathcal{E}_0 denotes the IR peak field strength, and $f(E)$ is the spectral amplitude in absence of the IR. The unknown two-IR-photon transition amplitudes are parameterized as $b_\beta(E) = c_\beta g(E - E_\beta)$. For g we use a Gaussian profile with a fixed width equal to the spectral width of the IR. The only adjustable parameters are the two-photon coupling strengths c_β , accounting for the different strengths of the transition into structured and unstructured continuum.

In Fig. 4 the cross-section Eq. (12) at $t_0 = -12$ IR opt.cyc. is compared to the TDSE result. The fringe separation of $2\pi/t_0$ discernable in Figs.1 and 4 proves that the structures are caused by interference of photo-

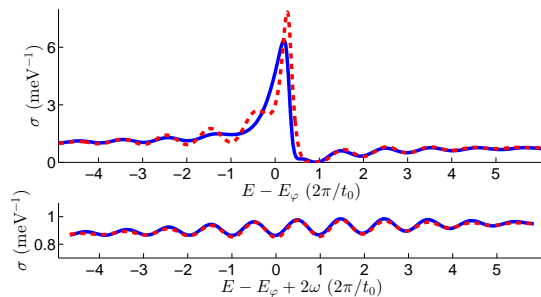


FIG. 4: Two-photon interference resonance in the $l = 1$ partial wave near E_φ (upper panel) and near $E_\varphi - 2\omega$ (lower). Cross-section Eq. (12) (dot-dashed) is compared to the full numerical result (solid) at $t_0 = -12$ opt.cyc.

electrons emitted at relative delay t_0 . Without any further adjustment of c_β or g the model equally well reproduces the spectra for varying intensities up to $I \lesssim 10^{12} \text{W/cm}^2$ and for all t_0 . The quadratic dependence on IR field strength \mathcal{E}_0 shows that this is a true two-photon process without resonant coupling to neighboring states. At short time-delays t_0 the effect is negligible, as fringe separation diverges and fringes are hardly discernable.

Turning now to the complementary channels for observing Fano line shapes by the IR field we calculate TAS near the $2snp$, $n \leq 6$ states using the pulse parameters of Ref. [9]. The spectra were determined from the full TDSE solutions following the method described in Ref. [19].

The delay dependence of the TAS differs from that of the PES: under the influence of the IR field the characteristic minimum of the Fano line all but disappears and does not fully reappear for delays shorter than the resonance life time. Fig. 5 shows as an example the computed transient absorption line of the $n = 4$ resonance at different IR delays. In all cases the numerical results conform with a generalized Fano line with a complex q

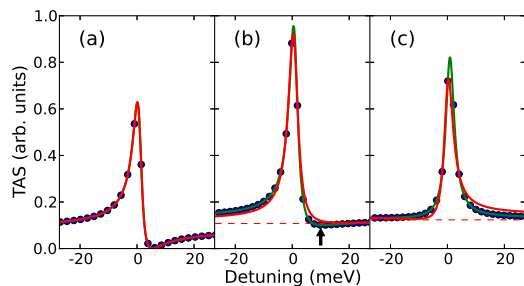


FIG. 5: TAS at the $2s4p$ resonance. Results are shown for (a) XUV only, (b) a 7 fs FWHM IR pulse with peak intensity $I = 2 \times 10^{12} \text{W/cm}^2$ reached at arrival of the XUV pulse, and (c) the peak IR intensity 5 fs after the XUV. Dots: numerical results; green lines: fit of a Fano profile with complex q (arrow marks the local minimum), solid red lines: Fano profile with real q according [9] and additional offset indicated by the dashed red line.

parameter. For comparison, we include the Fano shapes with the purely real q -parameter predicted in [9], where a constant pedestal of absorption was admitted to account for the offset of the lines from zero. The point to be noted is that the present numerical calculation is background-free, i.e., such a pedestal cannot be explained by a background contribution from other channels. The weak local minimum seen in the numerically computed absorption line at delay 0 corresponds to complex $q = -1.2 + i2.4$. This is at variance with real valued $q = -9$ resulting from the model proposed in [9]. Both, the offset from zero and the absorption minimum in the vicinity of the peak indicate that the influence of the control field is not fully captured by the model of [9].

The complex q in TAS and PES appears at parameters that are accessible by experimental setups as in Ref. [9]. For either observable the signature of complex q is a local minimum above 0. For PES the shape should follow Eq. (8), for TAS the exact shape can be obtained numerically. The main experimental difficulty obviously is the proper background subtraction. In case of the PES, the presence of the IR introduces a smooth background of partial waves, Eq. (2), in addition to the $l = 1$ partial wave that exhibits the Fano interference. However, at the times t_n where $\vec{\alpha} = 0$ the contributions from the other partial waves are negligible and $\Im(q)$ as given in the right panel in Fig. 3 is directly observable in the angle-integrated cross section. At other delays, the $l = 1$ cross section must be reconstructed from an angle-resolved measurement (see, e.g., [20]).

In summary, anomalous Fano profiles with complex q -parameter appear whenever a non-trivial relative phase between embedded state and continuum is imprinted on the system during the Fano decay. Such a phase can reflect internal dynamics of the embedded state $|\varphi\rangle$, i.e. when it is not strictly an eigenstate of a stationary Hamiltonian, as for decaying states and de-coherence. It can equally be generated by an external control, as demonstrated here. Our theoretical description of the process should be generalizable to systems where we can model the impact of the control on bound and embedded states and when control time is short compared to the resonance life time. This is the case for laser pulses on atoms or molecules, but the approach is also valid, e.g., for time-dependent electric or magnetic fields acting on quantum dots.

We acknowledge support by the excellence cluster “Munich Center for Advanced Photonics (MAP)” and by the Austrian Science Foundation project ViCoM (F41) and NEXTLITE (F049).

* Electronic address: armin.scrinzi@lmu.de
[1] U. Fano, Phys. Rev. **124**, 1866 (1961).

- [2] A. E. Miroshnichenko, S. Flach, and Y. S. Kivshar, *Rev. Mod. Phys.* **82**, 2257 (2010), URL <http://link.aps.org/doi/10.1103/RevModPhys.82.2257>.
- [3] K. Kobayashi, H. Aikawa, S. Katsumoto, and Y. Iye, *Phys. Rev. B* **68**, 235304 (2003), URL <http://link.aps.org/doi/10.1103/PhysRevB.68.235304>.
- [4] H.-W. Lee, *Phys. Rev. Lett.* **82**, 2358 (1999), URL <http://link.aps.org/doi/10.1103/PhysRevLett.82.2358>.
- [5] G. S. Agarwal, S. L. Haan, and J. Cooper, *Phys. Rev. A* **29**, 2552 (1984), URL <http://link.aps.org/doi/10.1103/PhysRevA.29.2552>.
- [6] M. Wickenhauser, J. Burgdoerfer, F. Krausz, and M. Drescher, *Phys. Rev. Lett.* **94**, 023002 (2005).
- [7] A. A. Clerk, X. Waintal, and P. W. Brouwer, *Phys. Rev. Lett.* **86**, 4636 (2001), URL <http://link.aps.org/doi/10.1103/PhysRevLett.86.4636>.
- [8] A. Bärnthaler, S. Rotter, F. Libisch, J. Burgdörfer, S. Gehler, U. Kuhl, and H.-J. Stöckmann, *Phys. Rev. Lett.* **105**, 056801 (2010), URL <http://link.aps.org/doi/10.1103/PhysRevLett.105.056801>.
- [9] C. Ott, A. Kaldun, P. Raith, K. Meyer, M. Laux, J. Evers, C. H. Keitel, C. H. Greene, and T. Pfeifer, *Science* **340**, 716 (2013).
- [10] Z. X. Zhao and C. D. Lin, *Phys. Rev. A* **71**, 060702 (2005), URL <http://link.aps.org/doi/10.1103/PhysRevA.71.060702>.
- [11] W.-C. Chu and C. D. Lin, *Phys. Rev. A* **87**, 013415 (2013).
- [12] J. Zhao and M. Lein, *New Journal of Physics* **14**, 065003 (2012).
- [13] W.-C. Chu, T. Morishita, and C. D. Lin, *Phys. Rev. A* **89**, 033427 (2014), URL <http://link.aps.org/doi/10.1103/PhysRevA.89.033427>.
- [14] L. Tao and A. Scrinzi, *New Journal of Physics* **14**, 013021 (2012).
- [15] A. Scrinzi, *New Journal of Physics* **14**, 085008 (2012), ISSN 1367-2630.
- [16] V. P. Majety, A. Zielinski, and A. Scrinzi, *New Journal of Physics* **17**, 063002 (2015), URL <http://stacks.iop.org/1367-2630/17/i=6/a=063002>.
- [17] M. Lewenstein, P. Balcou, M. Y. Ivanov, A. L'Huillier, and P. B. Corkum, *Phys. Rev. A* **49**, 2117 (1994).
- [18] *Supplemental material: derivation of eq. (8)*.
- [19] M. B. Gaarde, C. Buth, J. L. Tate, and K. J. Schafer, *Phys. Rev. A* **83**, 013419 (2011), URL <http://link.aps.org/doi/10.1103/PhysRevA.83.013419>.
- [20] G. A. Garcia, L. Nahon, and I. Powis, *Rev. Sci. Instrum.* **75**, 4989 (2004).

Supplemental Material: derivation of equation (8)

Alejandro Zielinski^a, Vinay Pramod Majety^a, Stefan Nagele^b,
 Renate Pazourek^b, Joachim Burgdörfer^b, and Armin Scrinzi^a
^a*Physics Department, Ludwig Maximilians Universität, D-80333 Munich, Germany and*
^b*Technische Universität Wien, A-1040 Vienna, Austria*
 (Dated: April 27, 2022)

For describing the action of the IR on the continuum we use the “strong field approximation”, where the field dominates the dynamics and continuum states are assumed to be unaffected by the scattering potential. Only the phase modification and momentum boost by the external dipole field is taken into account. The laser pulse is described through $\vec{A}(t)$, Eq. (2) of the main text, and t_1 denotes the end of the pulse where $\vec{A}(t_1) = 0$. In this approximation, the time-evolution in the IR dipole field from a state with momentum $\vec{k} - \vec{A}(t_0)$ at t_0 until the end of the pulse at t_1 , where it has the final momentum \vec{k} , is given as

$$U_{\text{IR}}|\vec{k} - \vec{A}(t_0)\rangle = e^{-i \int_{t_0}^{t_1} dt [\vec{k} - \vec{A}(t)]^2 / 2} |\vec{k}\rangle. \quad (1)$$

The effect of the IR on the embedded state is assumed to be a modification of its phase according to the Stark-shifted energy $E_\varphi(t) = E_\varphi + \Delta E_\varphi(t)$:

$$|\varphi, t_1\rangle = e^{-i \int_{t_0}^{t_1} dt [E_\varphi + \Delta E_\varphi(t)]} |\varphi, t_0\rangle. \quad (2)$$

If we neglect the coupling $V_{\vec{k}}$ between $|\varphi\rangle$ and $|\vec{k}\rangle$ for the duration of the IR, we can insert these time-evolutions into Eq. (4) of the main text to obtain the modification of the initial wave packet $|\psi_0\rangle$ by the IR pulse in the time interval from its creation by the XUV at t_0 until t_1

$$|\tilde{\psi}_1\rangle = |\varphi\rangle e^{-i \int_{t_0}^{t_1} dt [E_\varphi + \Delta E_\varphi(t)]} X_\varphi + \int d^3k e^{-i \int_{t_0}^{t_1} dt [\vec{k} - \vec{A}(t)]^2 / 2} |\vec{k}\rangle X_{\vec{k} - \vec{A}(t_0)}. \quad (3)$$

$|\tilde{\psi}_1\rangle$ equals the initial wavepacket $|\psi_1\rangle$ of Eq. (6) of the main text up to the overall phase $\exp\{-i \int_{t_0}^{t_1} dt [E_\varphi + \Delta E_\varphi(t)]\}$. As any global phase does not affect the crosssection, we will drop the distinction in the following steps. The dipole transition matrix element from an initial $l = 0$ state has the general form $X_{\vec{k}} = (\hat{\epsilon} \cdot \vec{k}) Z_{|\vec{k}|}$ for polarization direction $\hat{\epsilon}$. We neglect the $|\vec{k}|$ -dependence of $Z_{|\vec{k}|} \equiv Z$, as the resonance width Γ is very narrow compared to spectral width of $\sim 12 eV$ of an $0.15 fs$ XUV pulse, and also the energy dependence of the transition to the structureless continuum states $|\vec{k}\rangle$ far from threshold can be considered negligible across Γ .

We introduce the IR-induced offset $\vec{\alpha} := \int_{t_0}^{t_1} \vec{A}(t) dt$, define the polarization direction as the z -axis, and write the expansion of a plane wave into spherical Bessel functions j_l and Legendre polynomials P_l as

$$e^{ik\alpha \cos \theta_k} = \sum_l i^l (2l+1) P_l(\cos \theta_k) j_l(k\alpha), \quad (4)$$

where θ_k is the angle of \vec{k} with the z -axis.

We denote by $|Y_l^0\rangle$ the spherical harmonics for the spatial coordinates and assume $l = 1$ symmetry for $|\varphi\rangle = |Y_1^0\rangle |\varphi_1\rangle$. For the $l = 1$ partial wave of $|\psi_1\rangle$ one can perform the integration over angles of \vec{k}

$$|Y_1^0\rangle \langle Y_1^0 | \psi_1 \rangle = e^{-i(t_1-t_0)E_\varphi} |\varphi\rangle X_\varphi + \int dk k^2 e^{-i(t_1-t_0)k^2/2} |\vec{k}\rangle \sqrt{\frac{4\pi}{3}} k Z e^{-i\chi} \mathcal{J}(k), \quad (5)$$

where $|k\rangle = |Y_1^0\rangle \langle Y_1^0 | \vec{k}\rangle$ is the $l = 1$ partial wave of the continuum state and χ and \mathcal{J} are defined by Eqs. (9) and (10) of the main text.

The q -parameter for the modified wave-packet $|\psi_1\rangle$ replacing the initial wave packet $|\psi_0\rangle$ is

$$q_1 = \frac{1}{\pi V_{\vec{k}}^* k} \frac{\langle \Phi | \psi_1 \rangle}{\langle k | \psi_1 \rangle}. \quad (6)$$

with

$$|\Phi\rangle := |\varphi\rangle + \mathcal{P} \int k'^2 dk' |k'\rangle \frac{2V_{k'}^*}{k^2 - k'^2}, \quad (7)$$

compare Eq. (5) of the main text. In the evaluation of the principal value integral we neglect the k -dependence of \mathcal{J}

$$\mathcal{P} \int k'^2 dk' \frac{V_{k'}^*}{E_k - E_{k'}} \langle k' | \psi_1 \rangle \approx \mathcal{J}(k) e^{-\frac{i}{2} \int_{t_0}^{t_1} dt A^2(t)} \mathcal{P} \int k'^2 dk' \frac{V_{k'}^*}{E_k - E_{k'}} e^{-i(t_1 - t_0)k^2/2} \langle k' | \psi_0 \rangle. \quad (8)$$

Note that $\langle k' | \psi_0 \rangle = \frac{4\pi}{3} k' Z$. We find for the $l = 1$ component

$$q_1 = \frac{1}{\pi V_k^* k} \left\{ \frac{\langle \Phi | U_0 | \psi_0 \rangle}{\langle k | U_0 | \psi_0 \rangle} + \frac{\langle \varphi | U_0 | \psi_0 \rangle}{\langle k | U_0 | \psi_0 \rangle} [e^{-i\chi} / \mathcal{J}(k) - 1] \right\}. \quad (9)$$

U_0 is the free time-evolution during the time interval $[t_0, t_1]$ in absence of the IR and without the coupling $V_k \equiv 0$. It is given by $U_0 |k\rangle = e^{-i(t_0 - t_1)k^2/2} |k\rangle$ and $U_0 |\varphi\rangle = e^{-i(t_1 - t_0)E_\varphi} |\varphi\rangle$. The effect of U_0 on the q -parameter is negligible for time-intervals that are short compared to the decay time: $t_1 - t_0 \ll 1/\Gamma$:

$$\frac{\langle \Phi | \psi_0 \rangle}{\langle k | \psi_0 \rangle} \approx \frac{\langle \Phi | U_0 | \psi_0 \rangle}{\langle k | U_0 | \psi_0 \rangle} \quad \text{and} \quad \frac{\langle \varphi | \psi_0 \rangle}{\langle k | \psi_0 \rangle} \approx \frac{\langle \varphi | U_0 | \psi_0 \rangle}{\langle k | U_0 | \psi_0 \rangle}. \quad (10)$$

With this the first term can be identified with q_0 and we have obtained Eq. (8) of the main article.